


NANO EXPRESS

Open Access



# Antitumor Activity of Alloy and Core-Shell-Type Bimetallic AgAu Nanoparticles

Igor Shmarakov<sup>1\*</sup> , Luliia Mukha<sup>2</sup>, Nadiia Vityuk<sup>2</sup>, Vira Borschovetska<sup>1</sup>, Nelya Zhyshchynska<sup>1</sup>, Galyna Grodzyuk<sup>3,4</sup> and Anna Eremenko<sup>2</sup>

## Abstract

Nanoparticles (NPs) of noble metals, namely gold and silver, remain promising anticancer agents capable of enhancing current surgery- and chemotherapeutic-based approaches in cancer treatment. Bimetallic AgAu composition can be used as a more effective agent due to the synergetic effect. Among the physicochemical parameters affecting gold and silver nanoparticle biological activity, a primary concern relates to their size, shape, composition, charge, etc. However, the impact of metal components/composition as well as metal topological distribution within NPs is incompletely characterized and remains to be further elucidated and clarified. In the present work, we tested a series of colloidal solutions of AgAu NPs of alloy and core-shell type for an antitumor activity depending on metal molar ratios (Ag:Au = 1:1; 1:3; 3:1) and topological distribution of gold and silver within NPs ( $\text{Au}_{\text{core}}\text{Ag}_{\text{shell}}$ ;  $\text{Ag}_{\text{core}}\text{Au}_{\text{shell}}$ ). The efficacy at which an administration of the gold and silver NPs inhibits mouse Lewis lung carcinoma (LLC) growth in vivo was compared. The data suggest that in vivo antitumor activity of the studied NPs strongly depends on gold and silver interaction arising from their ordered topological distribution. NPs with Ag core covered by Au shell were the most effective among the NPs tested towards LLC tumor growth and metastasizing inhibition. Our data show that among the NPs tested in this study,  $\text{Ag}_{\text{core}}\text{Au}_{\text{shell}}$  NPs may serve as a suitable anticancerous prototype.

**Keywords:** Gold, Silver, Nanoparticles, Anticancer activity, Oxidative stress

**PACS:** 78.67.Bf (Nanocrystals, nanoparticles, and nanoclusters), 87.85.Rs (Nanotechnologies-applications), 87.85.em (Tissue damage)

## Background

Rapid advances in nanomedicine have generated an increasing number of potential diagnostic and therapeutic applications of nanoparticles in recent years [1, 2]. Among the different types of nanoparticles, metal nanoparticles including gold and silver have widespread use across the biomedical sciences [3, 4]. Nanoparticles (NPs) based on noble metals remain promising anticancer agents capable of enhancing existing surgery and chemotherapeutic-based approaches in cancer treatment. These NPs are being extensively used in a diagnostics and anticancer therapy due to intrinsic noble metal properties including ultramicroscopic size, large surface area-to-volume ratio, and consequently their

electronic and optical properties as well as high reactivity and stability [4]. In vitro and in vivo studies demonstrated that gold and silver NPs have strong antitumor activities [3, 5–7]. Bimetallic AgAu NPs are advantageous because they combine and resemble the unique properties of both gold and silver in one nanoparticle that are distinctly different from those inherent to individual components [1, 8]. Such physicochemical parameters as size, shape, composition, and charge greatly influence biological activity of NPs [9–12]. These properties of bimetallic AgAu NPs have been also shown to be advantageous in a development of aptamer-based biosensors [13]. However, many aspects of gold and silver NP-based systems remain unexplored, limiting the efficiency of their application. For instance, the impact of metal composition as well as metal topological distribution within NPs is incompletely characterized and remains to be further elucidated and clarified. An inclusion of different

\* Correspondence: igor.shmarakov@gmail.com

<sup>1</sup>Department of Biochemistry and Biotechnology, Yuriy Fedkovych Chernivtsi National University, Kotsyubynskiy St., 2, Chernivtsi 58012, Ukraine  
Full list of author information is available at the end of the article

metallic compositions has been shown to significantly affect reactive oxygen species (ROS) formation and has been suggested to be a major cause of different cellular disruptions and cell death enhancement observed in cells exposed to nanoparticles [12]. Our previous study demonstrated that combination of both gold and silver in one bimetallic NP confers advantageous biological activities and low toxicity in vivo [14]. In the present work, we test the ability of various bimetallic AgAu NPs to inhibit the metastatic tumor growth in vivo, employing mouse Lewis lung carcinoma (LLC) as a model. Aiming at expanding our knowledge on the AgAu nanoparticles biological activity, NPs were tested for an antitumor activity depending on metal molar ratios (Ag:Au = 1:1; 1:3; 3:1) and topological distribution of gold and silver within NPs ( $\text{Au}_{\text{core}}\text{Ag}_{\text{shell}}$ ;  $\text{Ag}_{\text{core}}\text{Au}_{\text{shell}}$ ). The data, revealed in the present study, emphasize that both parameters, metal molar ratio as well as metal topological distribution within bimetallic gold and silver nanoparticles, are critical features of NPs and can affect their antitumor activity. Among the NPs tested in this study,  $\text{Ag}_{\text{core}}\text{Au}_{\text{shell}}$  NPs may serve as the most suitable prototype for the development of an anticarcinomatous agent.

## Methods

### Nanoparticle Synthesis and Characterization

Colloidal solutions of bimetallic silver and gold NPs were obtained via chemical reduction of silver nitrate and tetrachlorauric acid ( $\text{AgNO}_3$  and  $\text{HAuCl}_4$ , Merck, Germany) with amino acid tryptophan (Trp, SC12-20120713, China). The components interacted in a molar ratio  $\text{Trp}:\text{M} = 2:1$ . The concentration of metal in the resulting solution was  $C(\text{M}) = 10^{-4}\text{M}$  followed by concentrating it to  $10^{-3}\text{M}$ . Bimetallic NPs of alloy type were obtained via simultaneous reduction of metal ions using initial metal molar ratios of Ag:Au = 3:1, 1:1, and 1:3, indicated as AgAu(3:1), AgAu(1:1), and AgAu(1:3) correspondingly. For the preparation of NPs of core-shell type with different topology, metal ions were reduced sequentially using the molar ratio Ag:Au = 1:1 and were indicated as  $\text{Au}_{\text{core}}\text{Ag}_{\text{shell}}$  and  $\text{Ag}_{\text{core}}\text{Au}_{\text{shell}}$ . For all colloids, the initial solutions of tryptophan were adjusted to  $\text{pH} = 10$ . Thus, amino acid was used in an anionic state that exists in alkaline medium. The pH control of the medium was performed using a pH meter I-160MI. As a working electrode, a glass electrode was used. Silver chloride electrode served as a reference one. Metals were injected into boiling solution of Trp followed by continuous heating of the reaction mixture.

The absorption spectra of the colloidal solutions of AgAu NPs were recorded in the UV-visible region with a spectrophotometer Lambda 35 (Perkin-Elmer, USA) in 1-cm quartz cells.

The size and morphology of nanoparticles were characterized with a transmission electron microscope (TEM) JEM-1230 (JEOL, Japan) with an accelerating voltage of 80 kV. One microliter of colloid was placed on carbon-coated copper grids and dried at room temperature. For the calculation of particle size distribution, the program ImageJ was used.

Scanning electron microscopy (SEM) was performed using a Tescan Mira 3 LMU microscope with an accelerating voltage of 5–20 kV. Energy-dispersive X-ray (EDX) spectra were taken using a built-in Oxford X-max 80  $\text{mm}^2$  setup.

The particle size distribution function was studied by a laser correlation spectrometer Zetasizer Nano S (Malvern, UK) equipped with a correlator (multicomputing correlator type 7032 ce) by a method based on the scattering of light on any micro-objects. The information signal from the random movement of nanoparticles was analyzed by multichannel spectrum analyzer and colorimeters; 1 ml of studied suspension was placed in a cylindrical optical glass cell with a diameter of 10 mm, which was located in a thermostated sample holder of a laser correlation spectrometer. Registration and statistical processing of the scattered laser light at  $173^\circ$  from the suspension (helium-neon laser LGN-111 was used with power output of 25 mW and wavelength of 633 nm) was performed three times during 120 s at  $25^\circ\text{C}$ . The resulting autocorrelation function was treated with standard computer programs PCS-Size mode v 1.61.

### Animal Husbandry and NP Administration

All the mice employed in our studies were congenic in the C57BL/6J genetic background. Male mice aged 12 weeks and weighing 18–20 g were used in the experiments. The animals were housed in cages containing a sterile paddy husk as bedding in a ventilated animal facility with a controlled temperature ( $21 \pm 2^\circ\text{C}$ ). All the mice were maintained on a laboratory complete diet with free access to water. As a model of malignant tumor growth, Lewis lung carcinoma (LLC) was employed. Tumor strain was kindly provided by the National Bank of Cell Lines from Human and Animal Tissues (R. E. Kavetsky Institute of Experimental Pathology, Oncology and Radiobiology, NAS of Ukraine). LLC transplantation was performed by intra-muscular injection into a femoral muscle of 0.2 ml 10% cell suspension in saline ( $3 \times 10^6$  cells/ml). Starting from day 5 after tumor cell inoculation (the moment of development of palpable tumors), the animals were randomly divided into groups receiving daily an intra-peritoneal injection of 100  $\mu\text{L}$  of the colloidal solution of NPs (either bimetallic alloy NPs with different metal molar ratios, where Ag:Au = 1:1, 1:3, and 3:1, and core-shell NPs with different topology  $\text{Au}_{\text{core}}\text{Ag}_{\text{shell}}$ ,  $\text{Ag}_{\text{core}}\text{Au}_{\text{shell}}$ ,

where Ag: Au = 1:1) at a dose of 500 µg/kg/day for 12 days. Control group of mice received an intraperitoneal injection of 100 µL of saline. General morphological parameters (animal weight, primary tumor size) and survival rate were monitored daily.

Twenty-four hours after the last NP injection (day 18 after tumor cells inoculation), the mice underwent euthanasia. At the time of sacrifice, mice were weighed, blood was taken from the inferior vena cava, and liver, lungs, and primary tumor were immediately removed. Blood serum was collected after centrifugation at 1500×g for 10 min. To isolate primary peripheral blood lymphocytes, the blood was first layered onto Ficoll-Paque (1.0777 g/ml; Pharmacia) and sedimented at 1000×g for 20 min at 21 °C. Mononuclear cells were harvested from the interface and pelleted three times in phosphate-buffered saline (PBS) without Ca<sup>2+</sup> and Mg<sup>2+</sup> to remove platelets (first at 650×g then twice at 235×g).

#### NP Antitumor Activity Analysis

Antitumor and antimetastatic activities of the NPs were evaluated on day 18 after tumor transplantation based on morphological parameters of primary tumor volume and number and size of lung metastases [15]. Primary tumor diameter was measured three times per week starting from day 5 after tumor inoculation. Tumor volume ( $V$ ) was calculated by the formula  $V = 0.52d^3$ , where  $d$  is the tumor diameter [15]. Anticancer activity was evaluated as tumor growth inhibition (TGI) rate calculated by the formula

$$\text{TGI} = \frac{V_0 - V_1}{V_0} \cdot 100\%,$$

where  $V_0$  and  $V_1$  are average tumor volumes in animals of a control and experimental group respectively.

The number and size of lung metastases were routinely analyzed using binocular microscope and millimeter scale. Lung metastasis inhibition (MI) index was calculated by a formula

$$\text{MI} = \frac{A_0 \cdot B_0 - A_1 \cdot B_1}{A_0 \cdot B_0} \cdot 100\%,$$

where  $A_0$  and  $A_1$  are metastasis frequencies in a control and experimental group and  $B_0$  and  $B_1$  are the average number of metastases in lungs of animals in a control and experimental group, respectively.

Subsequently, lung metastasis growth inhibition (MGI) index was calculated by a formula

$$\text{MGI} = \frac{S_0 - S_1}{S_0} \times 100\%,$$

where  $S_0$  and  $S_1$  are the average metastasis size in a control and experimental group, respectively.

#### Serum Lactate Dehydrogenase Activity

As a functional indicator for the monitoring of the activity of tumor growth and tissue infiltration rate, blood serum lactate dehydrogenase (LDH, EC 1.1.1.27) test was used. Lactate dehydrogenase enzymatic activity (IU/l) was determined in blood serum using commercially available kits (Felicity Diagnostics, Ukraine) according to manufacturer's protocol.

#### DNA Comet Assay

A single-cell DNA electrophoresis (DNA comet assay) was employed in order to assess NPs cytotoxicity towards mouse lymphocytes *in vivo*. Comet assay was performed exactly as described in [16]. Comets were visualized using a light microscope at ×400 magnification, and images were captured with a digital camera. Typically, 100 sequentially observed cells were analyzed per sample. Comet tail moment as a product of the tail length and the fraction of total DNA in the tail was then calculated automatically using *TriTek CometScore<sup>TM</sup>* software. Results were expressed as a percentage distribution of comets with a certain tail moment.

#### Oxidative Damage Product Measurement

The degree of oxidative modification of hepatic and primary tumor tissue proteins was assessed as previously described [14] through assessment of the levels of protein carbonylation and of protein sulfhydryl groups. Lipid peroxidation in hepatic and primary tumor tissue was determined by assessing the level of thiobarbituric acid-reactive substances (TBRAS).

#### Statistical Analysis

All data are presented as means ± S.D. Statistical comparisons involving treatment and control groups were first analyzed by a one-way ANOVA followed by multiple comparisons employing Tukey's HSD post hoc test.  $P$  values less than 0.05 were considered to be statistically significant.

## Results and Discussion

### Bimetallic Nanoparticles

Bimetallic AgAu nanoparticles were synthesized in the presence of the essential amino acid tryptophan as a reducing/stabilizing agent aiming to reduce toxicity of nanosized metals compared to those obtained in the presence of strong reducing agents and surfactants, as was previously demonstrated [14]. Tryptophan in an aqueous solution adjusted to high pH exists in anionic form having nonbonding pair of electrons on the nitrogen atom of the amino group and deprotonated carboxylic group  $-\text{COO}^-$ . These groups are involved in donor-acceptor bond formation with  $d$ -orbitals of the metal. During the synthesis of NPs, two competing processes

occur, donor-acceptor complex formation and metal reduction through indole ring. Thus, one molecule of Trp can serve as a bridge between NPs causing their aggregation. Reduction of the noble metal with tryptophan leads to the formation of large aggregates of NPs. To avoid such process, an excess of amino acid was used.

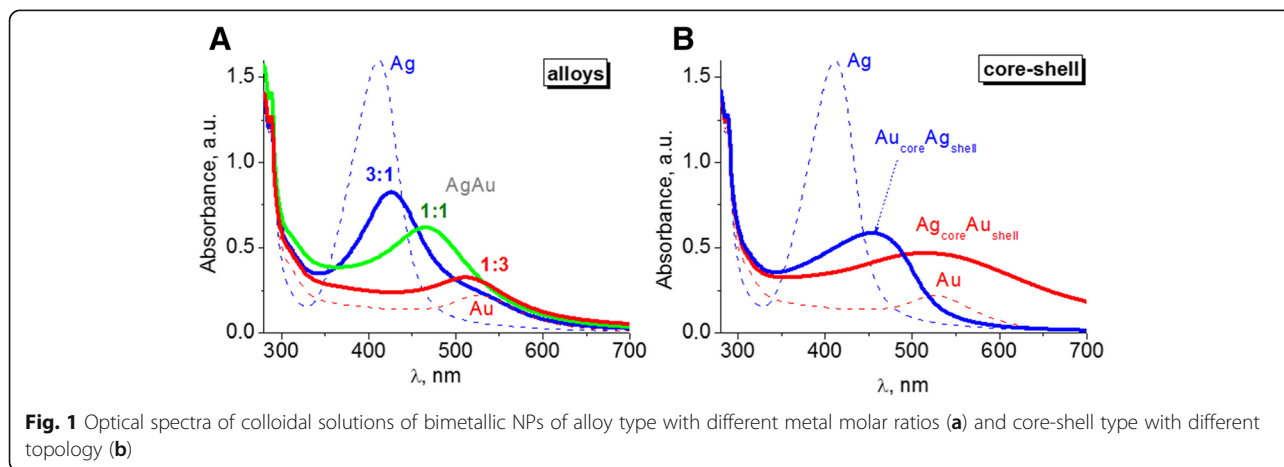
Colloidal solutions of obtained NPs had a bright color due to the localized surface plasmon resonance (LSPR) band absorption. Only one LSPR band is characteristic for bimetallic alloy NPs formed when  $\text{Ag}^+$  and  $[\text{AuCl}_4]^-$  ions are simultaneously reduced. Its maximum is located between the maxima inherent to the LSPR bands of individual metals (Fig. 1a) and is shifted from silver to gold with decreasing Ag:Au molar ratio. Namely, band maxima of AgAu NPs were observed at 427 nm for the ratio of 3:1, 466 nm for 1:1, and 511 nm for 1:3, between LSPR bands of individual metals obtained in the same experimental conditions at 411 nm for nanosized silver and 526 nm for gold.

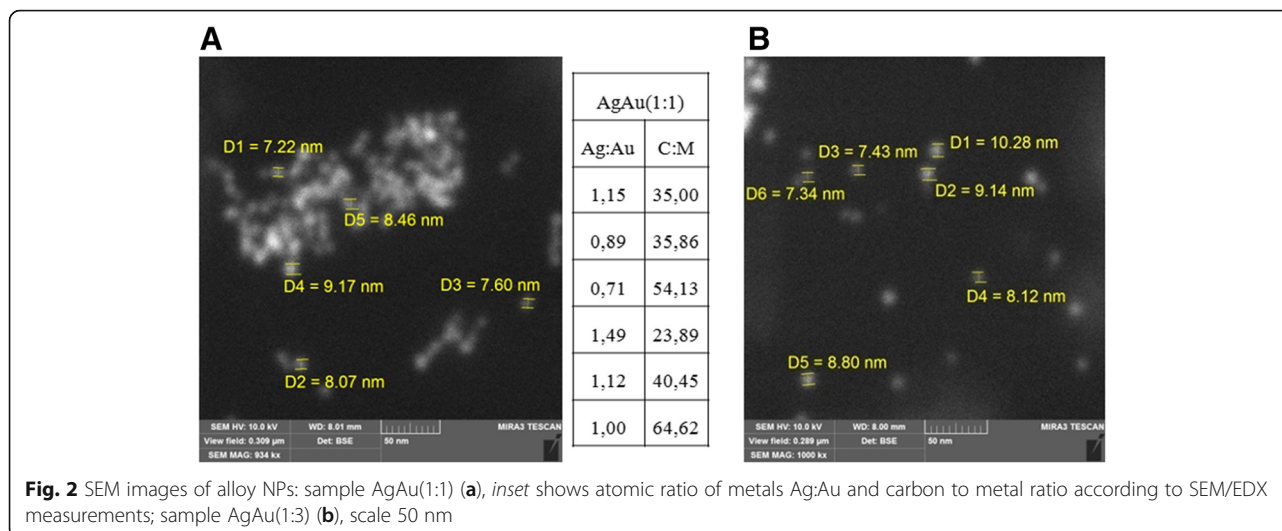
According to SEM images, the average size of AgAu NPs of alloy type was of 7–10 nm (Fig. 2a). We used elemental analysis to check the content of metals in obtained NPs. For the sample AgAu(1:1) studied with SEM/EDX, the Ag:Au ratio corresponds to a given experimental quantity. Namely, the average value shown in atomic % ratio was Ag:Au<sub>average</sub> = 1 (Fig. 2a, inset). Also, we fixed amount of carbon that was added to the mixture in the form of tryptophan. The experimental molar ratio Trp:M = 2:1 corresponds to atomic ratio C:M = 22:1, where C—carbon and M—metal. SEM/EDX showed that in the area of nanoparticles, carbon quantity exceeds a given number by several times, suggesting the accumulation of amino acid and its fragments around NPs, and thus forming an organic stabilizing shell.

Bimetallic core-shell NPs were synthesized by sequential reduction of metal ions. The disappearance of LSPR absorption band of previously formed monometallic particles, used as a core, and the growth of LSPR band of

the second metal in the spectra of the same colloid indicates the occurrence of new plasmonic metal shell. Such process is what we observed for both systems—previously formed silver core with a new gold shell and vice versa (Fig. 1b). High-intensive characteristic band of Ag NPs at 411 nm is screened by the absorption of gold nanoparticles at 515 nm. Also, LSPR band of Au NPs at 526 nm is covered by silver absorption with a maximum at 454 nm. Broad LSPR bands as well as their asymmetry indicate polydispersity and association of NPs of core-shell type in colloidal solutions. We suggest that it can be the aggregation of small NPs occurring due to cross-linking of particles through tryptophan during the synthesis. Polydispersity in colloids was evidenced by the dynamic light scattering (DLS) data (Fig. 3). Volume and intensity basis suggested the formation of a wide range of structures up to 300 nm in case of Au<sub>core</sub>Ag<sub>shell</sub>. And large aggregates up to 800 nm are characteristic for Ag<sub>core</sub>Au<sub>shell</sub>. At the same time, there are big fractions of small particles with an average diameter of 15 and 30 nm correspondingly.

The clear difference in topology of core-shell NPs is confirmed by TEM measurements. Au<sub>core</sub>Ag<sub>shell</sub> NPs are mainly spherical particles of 10–25 nm (Fig. 4) while their gold core (previously formed monometallic Au NPs) was smaller with the average size of 5–10 nm. Thus, as expected, the growth of the shell is accompanied by an increase of particle size. The same trend is characteristic for the system with silver core of 10–25 nm, and twice bigger Ag<sub>core</sub>Au<sub>shell</sub> NPs of 25–50 nm, but in this case, the shell is not uniform. According to TEM, the silver cores are mainly covered by small gold particles. The presence of small Au NPs of 5–10 nm in colloid presumably confirms that the formation of gold particles in the presence of tryptophan occurs simultaneously with the gold shell growth around Ag core due to fast reduction of gold with amino acid. Moreover, it causes an aggregation shown by TEM as well as by DLS.





### Antitumor Activity

An *in vivo* antitumor activity of the administered NPs was estimated based on the rate of primary tumor growth inhibition (TGI), lung metastasis growth inhibition (MGI), and metastasis inhibition (MI) indexes [15]. An inhibitory effect of NPs towards LLC primary tumor growth was observed for mice treated with NPs either with different Ag:Au molar ratio (AgAu(1:3), AgAu(1:1), AgAu(3:1)) or with different topology (Au<sub>core</sub>Ag<sub>shell</sub>, Ag<sub>core</sub>Au<sub>shell</sub>) (Table 1). Based on a primary tumor growth inhibition rate, all the administered NPs possessed an antitumor activity *in vivo*. For the majority of AgAu NPs administered, primary tumor growth inhibition was more than 30%. The maximum value (34%) of LLC primary tumor inhibition was attributed to NP with metal molar ratio as 1:3, AgAu(1:3) (Table 1).

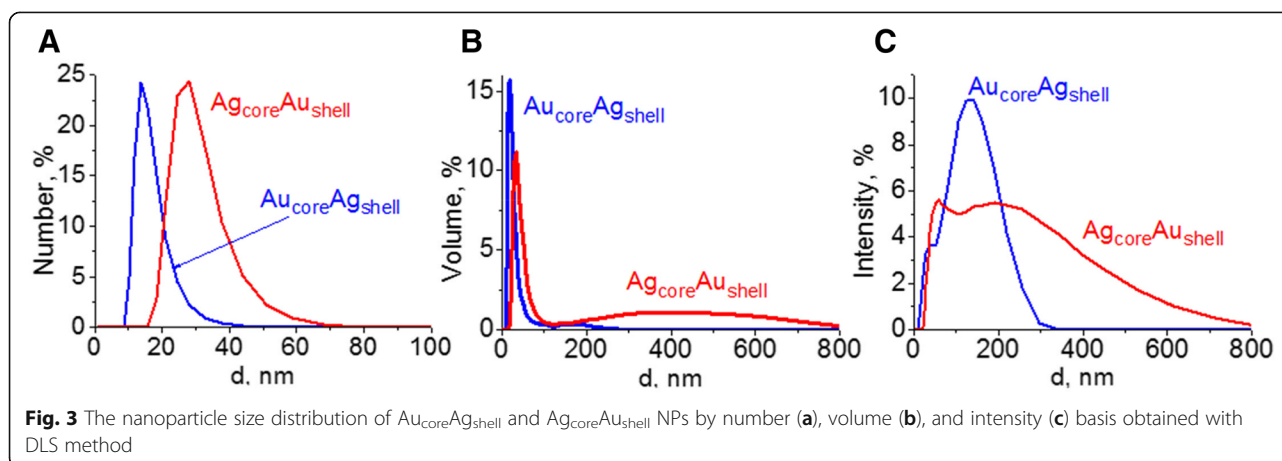
Despite a primary tumor growth inhibition, the administered NPs were not efficient in inhibiting of LLC lung metastases development. Metastasis inhibition (MI) index was calculated based on a frequency and a number of

metastatic nodes in mouse lungs. During the administration of AgAu(3:1) and Ag<sub>core</sub>Au<sub>shell</sub> NPs, MI index was 19 and 13%, respectively, whereas the treatment of mice with AgAu(1:3) (-28%), Au<sub>core</sub>Ag<sub>shell</sub> (-22%), and AgAu(1:1) (-10%) was characterized even by stimulation of metastasizing (Table 1).

Lung metastases were observed in mice of all the treatment groups. Lung metastasis growth inhibition index ranged from 4% (in AgAu(1:3)-treated group) to 27% (in Ag<sub>core</sub>Au<sub>shell</sub>-treated group). Conversely, the treatment with AgAu(3:1) NPs led to an accelerated metastasis growth in mice (MGI = -36%).

Thus, based on the parameters of primary tumor growth inhibition, lung metastasis growth inhibition, and metastasis inhibition index, it can be concluded that the highest antitumor activity was attributed to Ag<sub>core</sub>Au<sub>shell</sub> NPs (Table 1).

NPs administration to mice was accompanied with low serum lactate dehydrogenase (LDH) activity, an indicator of tumor growth activity and antitumor treatment



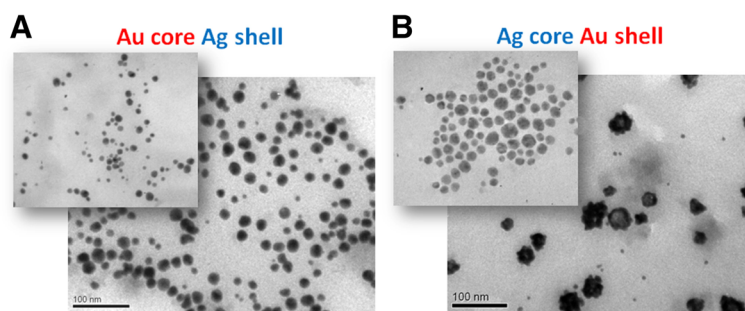


**Fig. 4** The TEM images of bimetallic NPs of core-shell type:  $\text{Au}_{\text{core}}\text{Ag}_{\text{shell}}$  (a) and  $\text{Ag}_{\text{core}}\text{Au}_{\text{shell}}$  (b). The insets show previously formed monometallic NPs applied as a core. Scale 100 nm

effectiveness [17]. For the mice with LLC that were not treated with NP, the level of serum LDH activity was more than 8500 IU/I (Fig. 5). As seen from the Fig. 5, NP administration led to a reduction of serum LDH activity supporting an observed inhibitory effect of NP administration towards tumor growth. The lowest value of LDH activity was detected in serum of mice treated with  $\text{Ag}_{\text{core}}\text{Au}_{\text{shell}}$  and  $\text{Au}_{\text{core}}\text{Ag}_{\text{shell}}$ . At the same time in the groups characterized with comparably higher primary tumor growth inhibition rates, serum LDH activity tended to be significantly lower. However,  $\text{AgAu}(3:1)$  NP administration had no significant effect on serum LDH activity in mice with LLC. This was consistent given the lowest primary tumor growth inhibition rate in this treatment group (Table 1, Fig. 5).

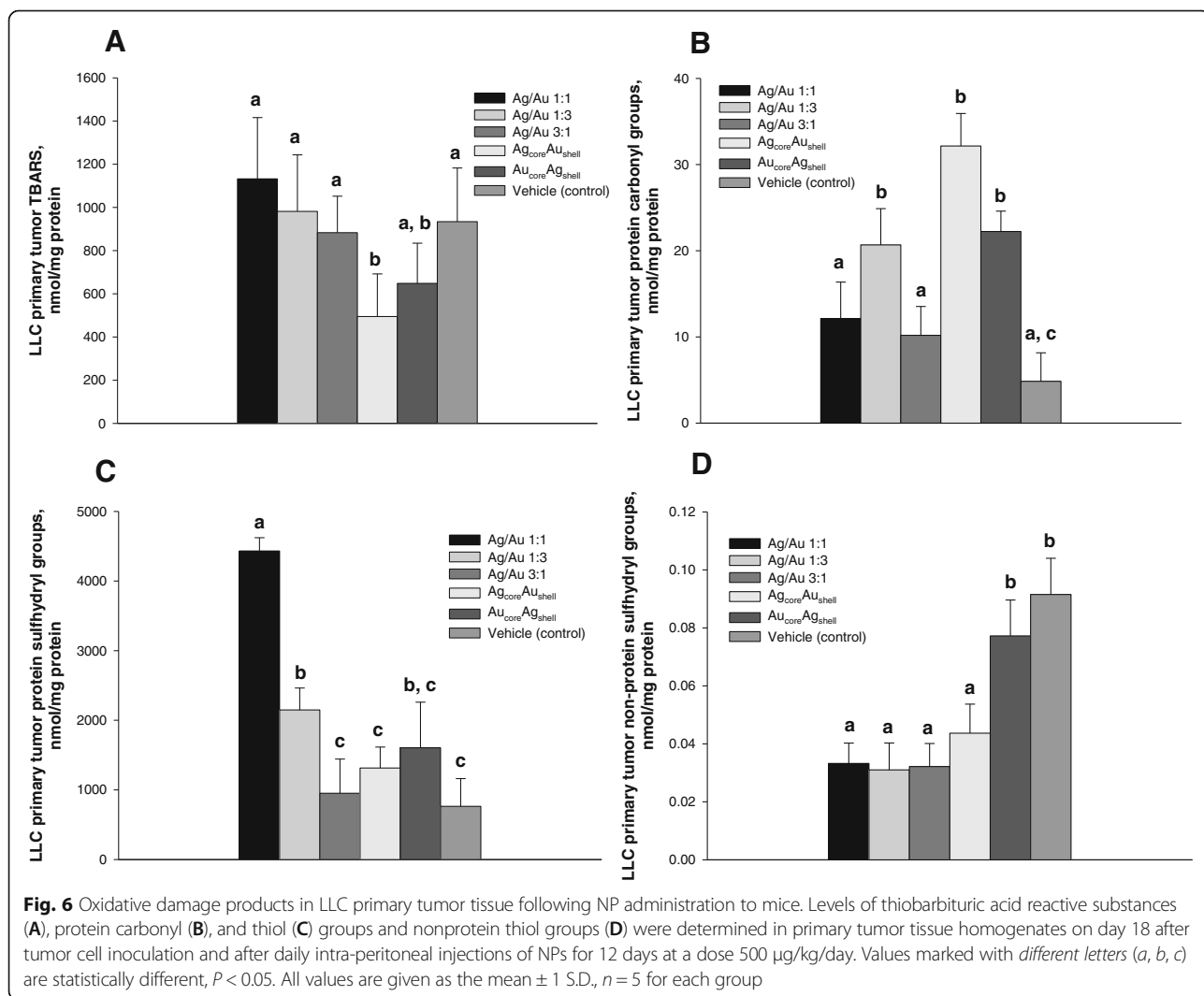
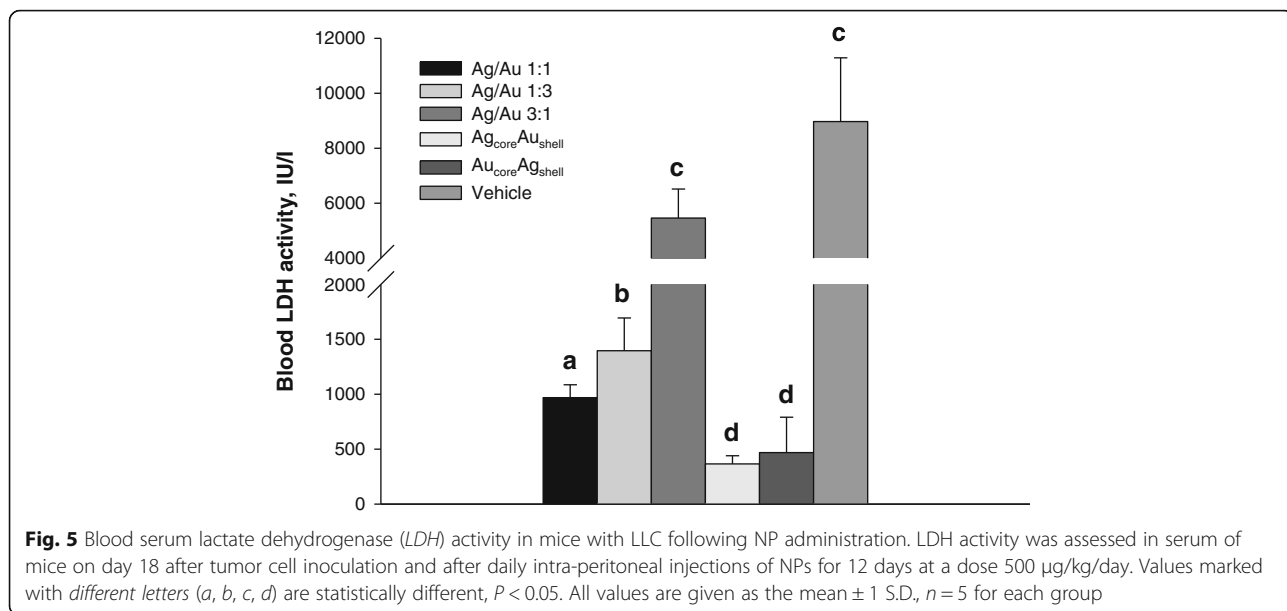
Oxidative stress within the cells is considered as one of the primary mechanisms underlying NP antitumor activity [18–20]. Silver and gold nanoparticles were reported to have an intrinsic property that allows a Fenton-type reaction to produce ROS [21, 22] with a subsequent lipid and protein oxidation, DNA damage, and cell death induction [23]. Several studies underscored a direct interaction between the ability of NPs to initiate ROS production and the subsequent cell death [2, 23]. Our results are consistent with this paradigm showing that administration of NPs resulted in oxidative stress induction in primary tumor tissue as was evidenced by accumulation of protein oxidation markers. However, based on the data, it can be concluded that only protein carbonylation may have an impact on primary tumor growth rates and metastasizing.

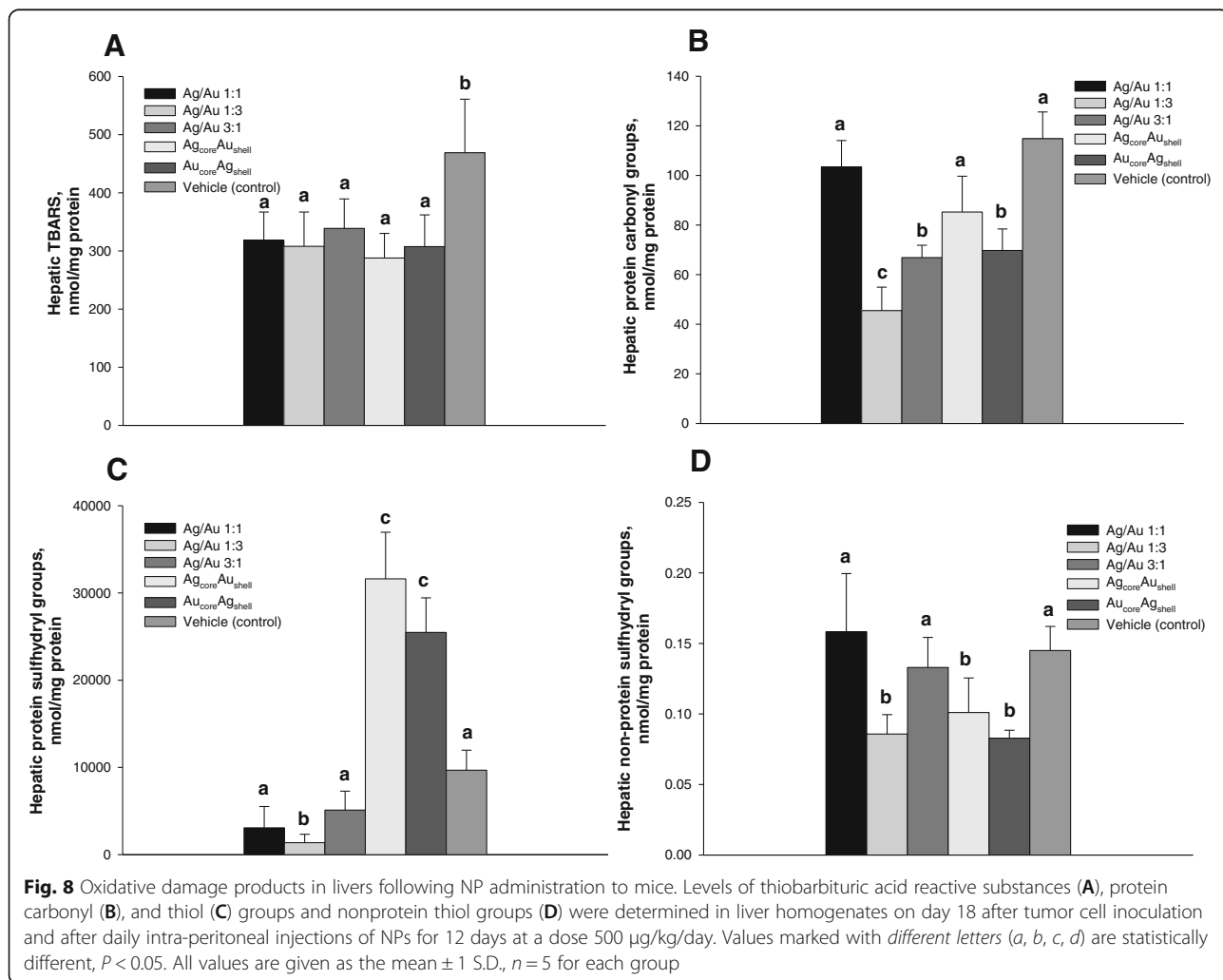
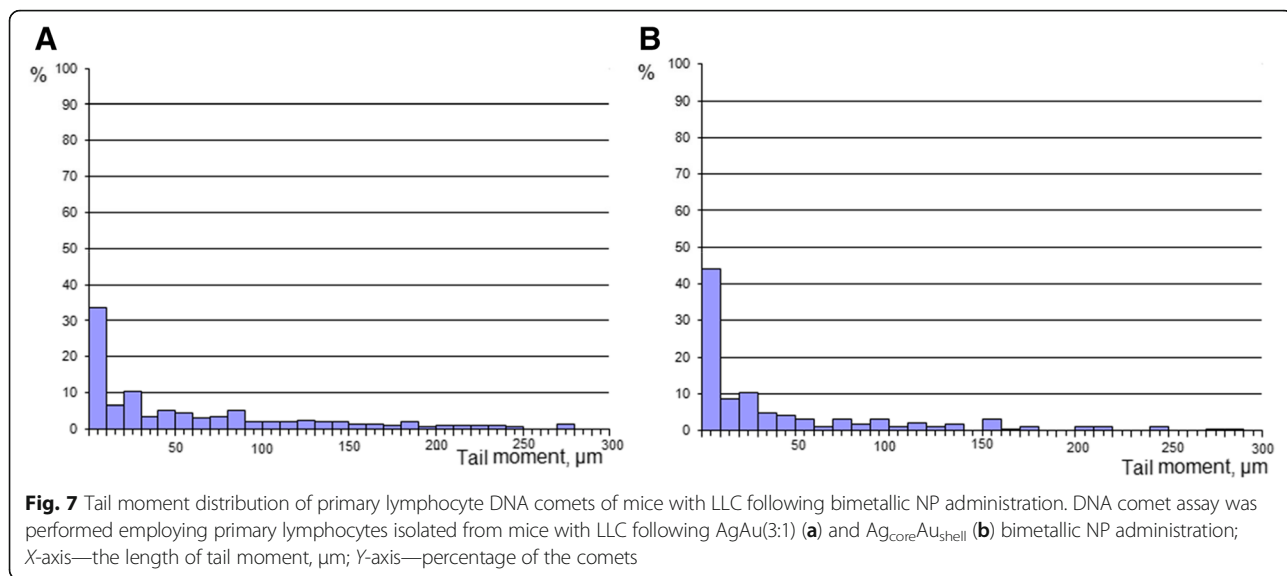
The analysis of oxidative processes intensity in the primary tumor tissue was performed by determining lipid and protein oxidative damage product accumulation. Consistent with morphological parameters of anti-tumor activity, we observed higher levels of oxidative damage product accumulation in primary tumor tissue of mice treated with NPs (Fig. 6). NP treatment did not accelerate lipid oxidation in the primary tumor (Fig. 6A), whereas led to higher protein oxidation (Fig. 6B). The administration of NPs with well-defined topology of metal components (either  $\text{Ag}_{\text{core}}\text{Au}_{\text{shell}}$  or  $\text{Au}_{\text{core}}\text{Ag}_{\text{shell}}$ ) was the most sufficient in inducing protein carbonylation in LLC primary tumor tissue. Conversely, the use of NPs with different metal molar ratios ( $\text{AgAu}(1:1)$  and  $\text{AgAu}(3:1)$ ) did not result in higher tumor protein carbonylation and did not affect or even cause elevation of primary tumor protein sulfhydryl groups (Fig. 6C). Unexpectedly, the action of NPs in case of  $\text{AgAu}(1:1)$ ,  $\text{AgAu}(1:3)$ , and  $\text{Au}_{\text{core}}\text{Ag}_{\text{shell}}$  was accompanied with even significantly higher levels of protein thiol groups. However, the administration of NPs, except for the  $\text{Au}_{\text{core}}\text{Ag}_{\text{shell}}$  NPs, resulted in significantly lower levels of nonprotein thiol groups in primary tumor tissue (Fig. 6D).

One of the major limitations of any substances with antitumor activity is a side effect expressed in cytotoxicity towards untransformed cells and tissues [20]. Since both therapeutic and toxic effects of nanoparticles need to be studied simultaneously, we have analyzed the ability of NPs to induce hepatic lipid and protein oxidation as well as lymphocyte DNA stability.

**Table 1** The indexes of antitumor activity of gold/silver bimetallic nanoparticles

Group	Type of nanoparticles	Primary tumor growth inhibition, %	Metastasis inhibition index, %	Lung metastasis growth inhibition, %
I	$\text{AgAu}(1:3)$	34	−28	4
II	$\text{AgAu}(1:1)$	33	−10	1
III	$\text{AgAu}(3:1)$	26	19	−36
IV	$\text{Au}_{\text{core}}\text{Ag}_{\text{shell}}$	32	−22	8
V	$\text{Ag}_{\text{core}}\text{Au}_{\text{shell}}$	31	13	27







Our attention was predominantly focused on Ag<sub>core</sub>Au<sub>shell</sub> NPs as these showed the highest antitumor activity. Ag<sub>core</sub>Au<sub>shell</sub> NPs upon their administration to mice with LLC possessed low in vivo genotoxicity towards untransformed cells as evidenced by single-cell DNA comet analysis of primary mouse lymphocytes (Fig. 7). The analysis of comet moment distribution revealed that up to 70% of cell population was characterized with intact integrated nuclear DNA after NPs administration. The percentage of cells with a damaged DNA (tail moment more than 150 μm) was only 10% (Fig. 7). Conversely, in a group of mice treated with AgAu(3:1) NPs, only 59% of the cells had intact nuclear DNA; 25% of the comets analyzed in this group had tail moment more than 150 μm, suggesting higher genotoxicity of these NPs towards lymphocytes.

All of the NPs administered in the present study did not lead to an increased hepatic lipid oxidation (Fig. 8A). After Ag<sub>core</sub>Au<sub>shell</sub> and Au<sub>core</sub>Ag<sub>shell</sub> NP treatment, the livers retained even higher protein sulfhydryl group levels (Fig. 8C), lower level of protein carbonylation (Fig. 8B) compared to the same parameters in the livers of untreated mice with LLC. These data suggest lower levels of oxidative damage in the livers of mice with LLC receiving NPs.

The data generated in the current study allow for concluding the presence of antitumor activity of bimetallic gold and silver NPs. Among the tested samples, and especially among the NPs with the same metal ratio of Ag: Au = 1:1 (alloy and core-shell type), NPs that consisted of Ag core covered by Au shell were the most active towards LLC tumor growth and metastasizing inhibition and possessed the lowest toxicity. Thus, the studied biological activity was the highest in case of ordered topological distribution of metal compounds within Ag<sub>core</sub>Au<sub>shell</sub> NPs, suggesting that in vivo antitumor activity of the studied NPs is strongly dependent on gold and silver interaction arising from their ordered topological distribution.

## Conclusions

Based on the parameters of primary tumor growth inhibition, lung metastasis growth inhibition, and metastasis inhibition index, the highest antitumor activity was attributed to Ag<sub>core</sub>Au<sub>shell</sub> NPs among the studied series of bimetallic nanoparticles with different metal content and topology. This was also confirmed by low serum lactate dehydrogenase activity compared to untreated mice with LLC and higher tumor tissue protein carbonylation. Ag<sub>core</sub>Au<sub>shell</sub> NPs showed low genotoxicity towards mouse lymphocytes as evidenced by DNA comet analysis and did not affect hepatic lipid and protein oxidation. Our data suggest that Ag<sub>core</sub>Au<sub>shell</sub> NPs used in this study may serve as a suitable prototype to develop anticarcinomatous agent and anticancer drug vehicle.

## Abbreviations

DLS: Dynamic light scattering; LDH: Lactate dehydrogenase; LLC: Lewis lung carcinoma; LSPR: Localized surface plasmon resonance; MGI: Metastasis growth inhibition; MI: Metastasis inhibition; NPs: Nanoparticles; ROS: Reactive oxygen species; TGI: Tumor growth inhibition; Trp: Tryptophan

## Authors' Contributions

AE and IS supervised this work and helped in the analysis and interpretation of the data. IM, NV, and GG carried out the synthesis of nanoparticles and their following characterization and analysis. VB and NZ performed the studies of antitumor activity and biochemical measurements. IS and IM worked on the drafting and revisions of the manuscript. All the authors have read and approved the final manuscript.

## Competing Interests

The authors declare that they have no competing interests.

## Publisher's Note

Springer Nature remains neutral with regard to jurisdictional claims in published maps and institutional affiliations.

## Author details

<sup>1</sup>Department of Biochemistry and Biotechnology, Yuriy Fedkovych Chernivtsi National University, Kotsuybyskiy St., 2, Chernivtsi 58012, Ukraine.

<sup>2</sup>Laboratory of Photonics of Nanosized Oxide Systems, Chuiko Institute of Surface Chemistry, National Academy of Sciences of Ukraine, General Naumov St., 17, Kyiv 03164, Ukraine. <sup>3</sup>L.V. Pisarzhevskii Institute of the Physical Chemistry, National Academy of Sciences of Ukraine, Kyiv, Ukraine.

<sup>4</sup>NanoMedTech LLC, Kyiv, Ukraine.

Received: 17 December 2016 Accepted: 26 April 2017

Published online: 04 May 2017

## References

1. Arvizo RR, Bhattacharyya S, Kudgus RA, Giri K, Bhattacharya R, Mukherjee P (2012) Intrinsic therapeutic applications of noble metal nanoparticles: past, present and future. *Chem Soc Rev* 41(7):2943–2970
2. Liu G, Li Q, Ni W, Zhang N, Zheng X, Wang Y et al (2015) Cytotoxicity of various types of gold-mesoporous silica nanoparticles in human breast cancer cells. *Int J Nanomedicine* 10:6075–6087
3. Bhattacharya R, Mukherjee P (2008) Biological properties of “naked” metal nanoparticles. *Adv Drug Deliv Rev* 60(11):1289–1306
4. Gheorghie DE, Cui L, Karmonik C, Brazdeikis A, Penalzoza JM, Young JK et al (2011) Gold-silver alloy nanoshells: a new candidate for nanotherapeutics and diagnostics. *Nanoscale Res Lett* 6:554
5. Loutfy SA, Al-Ansary NA, Abdel-Ghani NT, Hamed AR, Mohamed MB, Craik JD et al (2015) Anti-proliferative activities of metallic nanoparticles in an in vitro breast cancer model. *Asian Pac J Cancer Prev* 16(14):6039–6046
6. Mukherjee P, Bhattacharya R, Wang P, Wang L, Basu S, Nagy JA et al (2005) Antiangiogenic properties of gold nanoparticles. *Clin Cancer Res* 11(9):3530–3534
7. Chakraborty B, Pal R, Ali M, Singh LM, Shahidur Rahman D, Kumar Ghosh S et al (2016) Immunomodulatory properties of silver nanoparticles contribute to anticancer strategy for murine fibrosarcoma. *Cell Mol Immunol* 13(2):191–205
8. Holden MS, Nick KE, Hall M, Milligan JR, Chen Q, Perry CC (2014) Synthesis and catalytic activity of pluronic stabilized silver-gold bimetallic nanoparticles. *RSC Adv* 4(94):52279–52288
9. Hu M, Chen J, Li ZY, Au L, Hartland GV, Li X et al (2006) Gold nanostructures: engineering their plasmonic properties for biomedical applications. *Chem Soc Rev* 35(11):1084–1094
10. Millstone JE, Hurst SJ, Metraux GS, Cutler JJ, Mirkin CA (2009) Colloidal gold and silver triangular nanoprisms. *Small (Weinheim an der Bergstrasse, Germany)* 5(6):646–664
11. Samal AK, Polavarapu L, Rodal-Cedeira S, Liz-Marzan LM, Perez-Juste J, Pastoriza-Santos I (2013) Size tunable Au@Ag core-shell nanoparticles: synthesis and surface-enhanced Raman scattering properties. *Langmuir* 29(48):15076–15082
12. Mackey MA, Saira F, Mahmoud MA, El-Sayed MA (2013) Inducing cancer cell death by targeting its nucleus: solid gold nanospheres versus hollow gold nanocages. *Bioconjug Chem* 24(6):897–906

13. Hamidi-Asl E, Dardenne F, Pilehvar S, Blust R, De Wael K (2016) Unique properties of core shell Ag@Au nanoparticles for the aptasensing of bacterial cells. *Chemosensors* 4(3):16
14. Shmarakov IO, Mukha IP, Karavan W, Chunikhin OY, Marchenko MM, Smirnova NP, et al. Tryptophan-assisted synthesis reduces bimetallic gold/silver nanoparticle cytotoxicity and improves biological activity. *Nanobiomedicine*. 2014;1(6). doi:10.5772/59684.
15. Pyaskovskaya ON, Kolesnik DL, Fedorchuk AG, Prokhorova IV, Solyanik GI (2016) 2-Deoxy-D-glucose enhances dichloroacetate antitumor action against Lewis lung carcinoma. *Exp Oncol* 38(3):176–180
16. Kamins'kyi VO, Lutsyk MD, Stoika RS (2005) Comet assay of DNA fragmentation: modification of silver staining for obtaining permanent preparations. *Ukrains'kyi Biokhimichnyi Zhurnal* (1999) 77(6):105–108
17. Faloppi L, Del Prete M, Casadei Gardini A, Santini D, Silvestris N, Bianconi M et al (2016) The correlation between LDH serum levels and clinical outcome in advanced biliary tract cancer patients treated with first line chemotherapy. *Scientific Reports* 6:24136
18. Manke A, Wang L, Rojanasakul Y (2013) Mechanisms of nanoparticle-induced oxidative stress and toxicity. *Biomed Res Int* 2013:942916
19. Pal R, Chakraborty B, Nath A, Singh LM, Ali M, Rahman DS et al (2016) Noble metal nanoparticle-induced oxidative stress modulates tumor associated macrophages (TAMs) from an M2 to M1 phenotype: an in vitro approach. *Int Immunopharmacol* 38:332–341
20. Yamada M, Foote M, Prow TW (2015) Therapeutic gold, silver, and platinum nanoparticles. *Wiley Interdisciplinary Rev Nanomed Nanobiotechnol* 7(3):428–445
21. Sang Y, Zhang L, Li YF, Chen LQ, Xu JL, Huang CZ (2010) A visual detection of hydrogen peroxide on the basis of Fenton reaction with gold nanoparticles. *Anal Chim Acta* 659(1–2):224–228
22. Navalon S, de Miguel M, Martin R, Alvaro M, Garcia H (2011) Enhancement of the catalytic activity of supported gold nanoparticles for the Fenton reaction by light. *J Am Chem Soc* 133(7):2218–2226
23. Dutta D, Sahoo AK, Chattopadhyay A, Ghosh SS (2016) Bimetallic silver nanoparticle-gold nanocluster embedded composite nanoparticles for cancer theranostics. *J Mater Chem B* 4(4):793–800

Submit your manuscript to a SpringerOpen<sup>®</sup> journal and benefit from:

- Convenient online submission
- Rigorous peer review
- Immediate publication on acceptance
- Open access: articles freely available online
- High visibility within the field
- Retaining the copyright to your article

---

Submit your next manuscript at ► [springeropen.com](http://springeropen.com)

---